Energy Engineering

Tech Science Press

DOI: 10.32604/ee.2022.015504

ARTICLE

HCl-Induced Hg^0 Transformation over $CuMn_2O_4$ Sorbent

Aijia Zhang, Yingju Yang, Jing Liu* and Junyan Ding

State Key Laboratory of Coal Combustion, School of Energy and Power Engineering, Huazhong University of Science and Technology, Wuhan, 430074, China

*Corresponding Author: Jing Liu. Email: liujing27@mail.hust.edu.cn

Received: 23 December 2020 Accepted: 21 May 2021

ABSTRACT

$CuMn_2O_4$ spinel has been regarded as a highly efficient sorbent for Hg^0 capture from flue gas. The regenerability and recyclability of $CuMn_2O_4$ sorbent are mainly associated with the mercury speciation adsorbed on its surface. However, the effect mechanism of HCl on Hg^0 transformation over $CuMn_2O_4$ sorbent is still elusive. Experiments were conducted to understand the effect of HCl on Hg^0 transformation over $CuMn_2O_4$ sorbent. The results indicate that $CuMn_2O_4$ sorbent is a mesoporous material and possesses a good thermal stability. $CuMn_2O_4$ shows >95% Hg^0 removal efficiency in a wide temperature window of 50–350°C. The favorable electron-transfer environment caused by the mixed valence states of Cu and Mn cations is responsible for the excellent Hg^0 removal performance of $CuMn_2O_4$ sorbent. $CuMn_2O_4$ shows a higher Hg^0 adsorption capacity of 4774.57 μg/g. Hg^0 adsorption process over $CuMn_2O_4$ sorbent can be well described by the developed kinetic model. Hg^0 removal efficiency of $CuMn_2O_4$ sorbent does not depend on the presence of HCl. Mercury species adsorbed on the $CuMn_2O_4$ sorbent in the presence of HCl mainly exist in the forms of HgO and $HgCl_2O_8 \cdot H_2O$. HCl shows a significant effect on mercury speciation over $CuMn_2O_4$ sorbent. Most of HgO species will be transformed into $HgCl_2O_8 \cdot H_2O$ in the presence of HCl.

KEYWORDS

$CuMn_2O_4$; mercury; HCl; sorbent; electron transfer

1 Introduction

Mercury is a toxic air pollutant with high volatility, and is harmful to human health and ecosystem [1–5]. Thermal power plant is considered to be a main source of gaseous anthropogenic mercury emissions in China [6–8]. The Minamata Convention on Mercury has officially come into force in August 2017 to restrict the global anthropogenic mercury emissions [9]. In order to meet the requirements of the Minamata Convention on Mercury, the mercury emission limit of thermal power plants in China will be set to 1 $\mu g/m^3$ in 2030 [10]. Therefore, mercury emission control in thermal power plants becomes increasingly urgent.

To date, mercury emission control technologies of thermal power plants mainly include: sorbent injection [11–16], catalytic oxidation [17–20] and bromide addition [21–23]. The technical strategy of catalytic oxidation and bromide addition is to oxidize Hg^0 into Hg^{2+}, which

This work is licensed under a Creative Commons Attribution 4.0 International License, which permits unrestricted use, distribution, and reproduction in any medium, provided the original work is properly cited.

is subsequently removed by the wet flue gas desulfurization equipment. However, Hg^{2+} may be reduced to Hg^0 in the wet desulfurization solution [24], leading to the secondary mercury pollution [25]. Therefore, sorbent injection is considered as an effective mercury emission control technology [26,27]. Currently, bromine-modified activated carbon is the commercial mercury sorbent. However, there are some problems during the application of activated carbon [28], such as high price, adverse effects on the quality of fly ash as the cement raw material, and non-recyclable utilization. Therefore, it is necessary to develop the cost-effective and regenerable mercury sorbents.

Currently, copper-manganese spinel oxide has received more and more attention due to its unique structure and physical-chemical properties [29]. Copper-manganese oxide has been widely used in the field of catalysis, such as CO oxidation [30], water-gas shift reaction [31], and pollutant removal [32]. The excellent catalytic activity of copper-manganese oxide is closely related to the flexible valence states of $Cu^{+/2+}$ and $Mn^{2+/3+/4+}$ [33]. The valence state changes of copper and manganese cations easily lead to an electron-transfer environment [34], which is beneficial to the adsorption and oxidation of Hg^0. Therefore, our previous work synthesized copper-manganese spinel-type oxide and used to remove Hg^0 from simulated flue gas (4% O_2 + 12% CO_2 + N_2) [35–37]. HCl usually exists in flue gas, and has a great influence on the mercury transformation [38]. However, to date, no relevant research has been reported to investigate the effects of HCl on Hg^0 transformation over $CuMn_2O_4$ sorbent.

In this work, the thermogravimetric (TG) analysis, BET specific surface area, and pore size distribution were used to evaluate the thermal stability and textural properties of $CuMn_2O_4$ sorbent. The effect of HCl on Hg^0 transformation over $CuMn_2O_4$ sorbent was systematically investigated. The related effect mechanism was clarified based on the temperature-programmed desorption (TPD) analysis. This study can provide a theoretical basis for the application of $CuMn_2O_4$ sorbent.

2 Experimental Methods

2.1 Sorbent Synthesis and Characterization

$CuMn_2O_4$ sorbent was synthesized by our previously proposed low-temperature sol-gel auto-combustion synthesis method [35]. The detailed synthesis procedure has been provided in our previous work [35]. The thermal stability of sorbent was evaluated on a thermogravimetric analyzer (TA SDT-Q600). The temperature was increased from 25 to 850°C in the air atmosphere at a heating rate of 10 °C/min. The flow rate of air was set as 100 mL/min. The textural properties (such as specific surface area and pore size distribution) were investigated on a N_2 physical adsorption apparatus (ASAP2020, Micromeritics). Sorbents were degassed at 200°C for 2 h before the N_2 adsorption experiments.

2.2 Hg^0 Removal Experiments

The Hg^0 removal experiments were carried out in a fixed-bed reactor system, including a gas feed subsystem, a Hg^0 generation subsystem, a quartz reactor, and an online mercury analyzer (VM3000, Mercury Instruments, Germany). The simulated flue gas (including 4% O_2, 12% CO_2, 0–10 ppm HCl, and N_2 as the balance gas) were fed into the quartz reactor. In order to avoid the interference of other gas components (such as NO, SO_2, and H_2O) in the study of the effect mechanism of HCl on Hg^0 transformation, these gas components were not included in the simulated flue gas. The total flow rate of the simulated flue gas was 1 L/min. Stable Hg^0 vapor was continuously generated from a mercury permeation tube, and was fed into the simulated flue

gas by N_2. Hg^0 concentration in the flue gas was maintained at 90 $\mu g/m^3$. 0.2 g of sorbent was mixed with 1.8 g of quartz sand to reduce the pressure drop of flue gas through the sorbent bed and to prevent pipeline blockage. The height of sorbent bed was 19 mm, and the gas hourly space velocity (GHSV) was 5×10^4 h^{-1}. Before the flue gas entering the mercury analyzer, the acid gas HCl was removed by a 10% NaOH solution to prevent the HCl corrosion of mercury measurement instrument. The experimental details have been clearly described in our previous work [35].

3 Results and Discussion

3.1 Characterization Analysis

3.1.1 TGA Analysis

Thermogravimetric analysis was used to investigate the thermal stability of $CuMn_2O_4$ sorbent. The TG and DTG curves of $CuMn_2O_4$ spinel in air atmosphere are displayed in Fig. 1. It can be seen that the weight of sorbent decreases slightly when the temperature increases and the weight loss curve of $CuMn_2O_4$ is flat. As the temperature increased from 25 to 350°C (the maximum temperature of Hg^0 removal experiments), the weight loss was 0.61%, as shown in Fig. 1a. A small weight loss of 0.17% was obtained when the temperature further increased from 350 to 850°C. Differential thermogravimetric (DTG) curve was used to calculate weight loss rates, as shown in Fig. 1b. $CuMn_2O_4$ sorbent showed three endothermic peaks at 498, 583 and 825°C. Moreover, two exothermic peaks were also observed at 527 and 628°C. The largest weight loss rate of $CuMn_2O_4$ (0.0084%/min) occurs at 583°C. Obviously, these results indicate that $CuMn_2O_4$ sorbent has a good thermal stability at high temperatures.

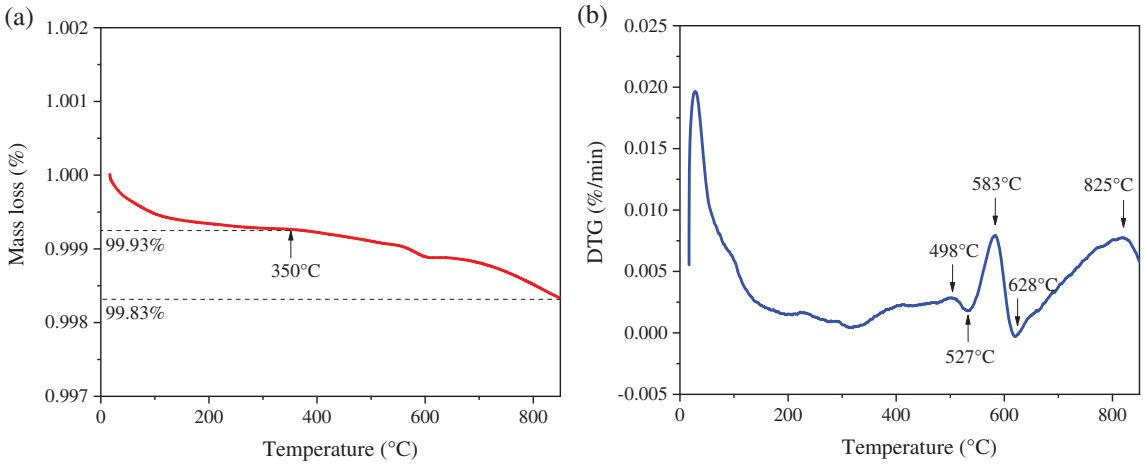

Figure 1: TG-DTG curves of $CuMn_2O_4$ sorbent: (a) TG curve and (b) DTG curve

3.1.2 BET Surface Area and Pore Size Distribution

The BET surface area and pore size distribution were measured to understand the textural properties of $CuMn_2O_4$ sorbent. The N_2 adsorption-desorption isotherms and pore size distribution of $CuMn_2O_4$ sorbent is shown in Fig. 2. According to the physical adsorption isotherm classification proposed by the International Union of Pure and Applied Chemistry (IUPAC), the N_2 adsorption-desorption isotherm of $CuMn_2O_4$ sorbent is the type IV curve (Fig. 2a). There is an obvious hysteresis loop in the relative pressure range of 0.60–0.95, which is the typical feature

of mesopores. The pore size of $CuMn_2O_4$ sorbent is mainly distributed in the range of 5–50 nm, suggesting the existence of mesoporous structure. The BET surface area, average pore size, and pore volume are 29.33 m^2/g, 24.85 nm, and 0.18 cm^3/g, respectively. Pores with a size between 2–50 nm are defined as mesopores [39]. Therefore, $CuMn_2O_4$ sorbent is a mesoporous material, which is favorable for the mass transfer during Hg^0 capture.

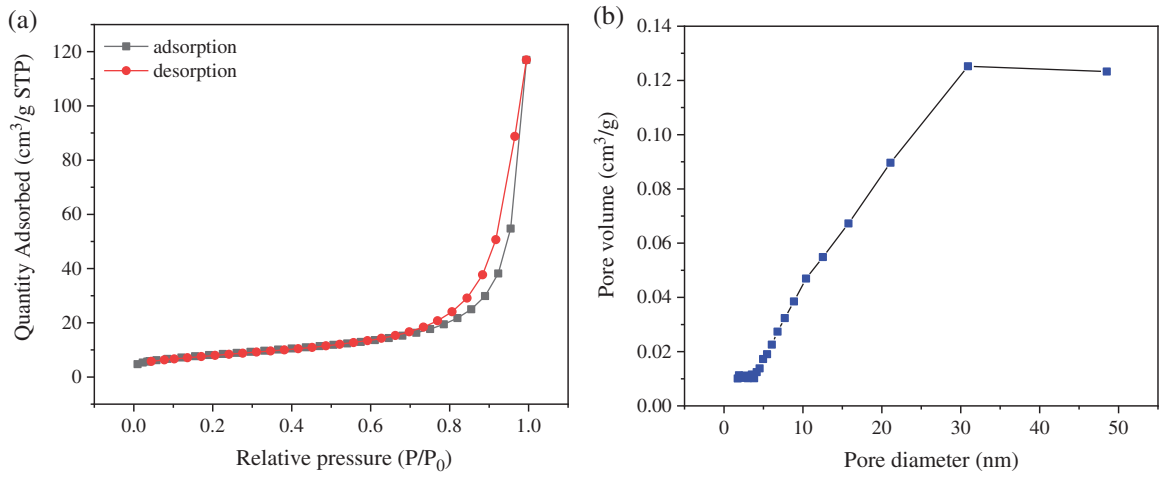

Figure 2: (a) N_2 adsorption-desorption isotherms; (b) Pore size distribution of $CuMn_2O_4$ sorbent

3.2 Mercury Removal Performance

3.2.1 Removal Efficiency

The mercury removal efficiency of $CuMn_2O_4$ sorbent in the temperature range of 50–350°C is shown in Fig. 3. It can be seen that $CuMn_2O_4$ sorbent shows >95% Hg^0 removal efficiency over the wide temperature range. The excellent Hg^0 removal efficiency may be attributed to the high concentrations of surface Cu atom and chemisorption oxygen. The XPS analysis of our previous work [35] found that the surface Cu and Mn atoms exist in the form of flexible valence (Cu^+, Cu^{2+}, Mn^{2+}, Mn^{3+}, and Mn^{4+}). A part of Cu^+ cations occupied the tetrahedral position of $CuMn_2O_4$ spinel, and some Mn^{4+} cations were located at the octahedral position of $CuMn_2O_4$ spinel. Thus, the different valence states and position distributions of metal cations (Cu^+, Cu^{2+}, Mn^{2+}, Mn^{3+} and Mn^{4+}) leaded to lattice distortion of $CuMn_2O_4$ spinel, resulting in an electron-transfer environment which can accelerate Hg^0 adsorption and oxidation over $CuMn_2O_4$ sorbent. Therefore, $CuMn_2O_4$ sorbent exhibits excellent Hg^0 removal performance in a wide temperature window.

3.2.2 Adsorption Kinetics

A mathematical model is an effective tool to predict the Hg^0 adsorption capacity of sorbent and to evaluate the performance of sorbent for mercury removal under different operating conditions [9]. The mathematical model can provide a rational basis for describing and characterizing the effectiveness of sorbent injection for mercury removal. In addition, the mathematical model can provide theoretical guidance for the development of new sorbents and for the optimization of sorbent injection process. Therefore, it is necessary to study the adsorption kinetics of mercury on the sorbent surface.

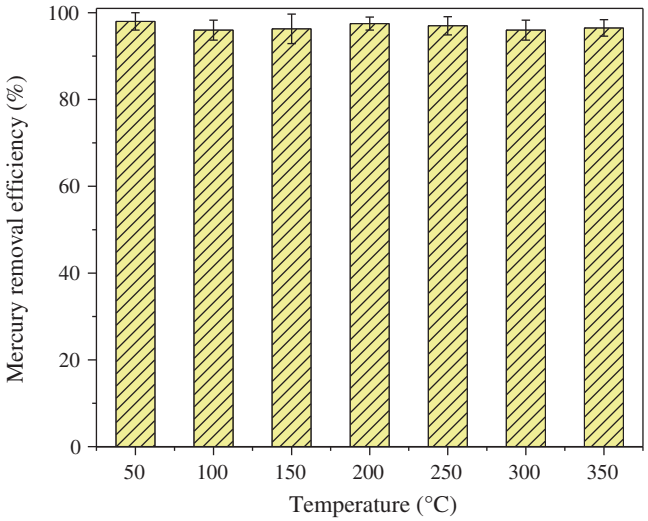

Figure 3: Hg^0 removal efficiency of $CuMn_2O_4$ sorbent at 50–350°C [35]

In a fixed-bed reactor, as the flue gas flows through a constant-temperature sorbent bed, the differential mass conservation equation of mercury can be described as:

$$u\frac{\partial C}{\partial z}+\frac{\partial C}{\partial t}+\frac{1-\varepsilon}{\varepsilon}\frac{\partial q}{\partial t}=D_{\mathrm{ax}}\frac{\partial^2 C}{\partial z^2} \tag{1}$$

where u represents the flow velocity of flue gas. C represents the Hg^0 concentration in the flue gas. ε represents the porosity of sorbent bed. q represents the Hg^0 adsorption capacity of sorbent. D_{ax} represents the axial diffusion coefficient. z represents the axial coordinate. t represents time. The differential mass conservation equation is closely related to the constitutive equation of Hg^0 adsorption rate on the sorbent.

It was reported that the axial diffusion of mercury can be ignored if the ratio of the sorbent bed diameter (d_{bed}) to the sorbent particle diameter (d_{particle}) is greater than 35 and the ratio of the sorbent bed thickness (h_{bed}) to the sorbent particle diameter is greater than 75 [27]. In this work, $d_{\mathrm{bed}}/d_{\mathrm{particle}}$ and $h_{\mathrm{bed}}/d_{\mathrm{particle}}$ are 120 and 253, respectively. In addition, the Hg^0 removal experiments were conducted under the condition of a larger flue gas flow rate of 1000 mL/min. These indicated that Hg^0 removal process of $CuMn_2O_4$ sorbent is controlled by reaction kinetics. The chemisorption mechanism is responsible for Hg^0 adsorption over $CuMn_2O_4$ sorbent. The chemical adsorption reaction has been incorporated into the mathematical model (i.e., Langmuir isotherm equation) of adsorption kinetics. Therefore, the mass diffusion resistance of mercury in the sorbent particle and the external boundary layer can be ignored. The Langmuir isotherm equation can be used to describe the adsorption process of Hg^0 on the $CuMn_2O_4$ surface:

$$\frac{dq}{dt}=k_{\mathrm{a}}C_{\mathrm{in}}(q_e-q) \tag{2}$$

where k_{a} represents the rate constant of Hg^0 adsorption on the sorbent surface. C_{in} represents the stable Hg^0 concentration in the flue gas at the inlet of the fixed bed reactor. q_e represents

the equilibrium Hg^0 adsorption capacity of $CuMn_2O_4$ sorbent. q represents the Hg^0 adsorption capacity at time t. Integrating Eq. (2), q can be expressed as:

$$q = q_e(1 - \exp(-k_a C_{in} t)) \tag{3}$$

k_1 is used to replace $k_a C_{in}$, Eq. (3) can be expressed as:

$$q = q_e(1 - \exp(-k_1 t)) \tag{4}$$

The increment of Hg^0 adsorption amount on the sorbent surface within the time range of Δt can be calculated by the following formula:

$$\Delta q = \frac{Q}{m}(C_{in} - C_{out}(t))\Delta t \tag{5}$$

where Q represents the flow rate of flue gas. m represents the weight of sorbent. $C_{out}(t)$ represents the Hg^0 concentration in the flue gas at the reactor outlet at time t. During the whole Hg^0 adsorption experiment, Hg^0 adsorption amount of sorbent can be expressed as:

$$q = \int_m^t \frac{Q}{m}(C_{in} - C_{out}(t))dt \tag{6}$$

In this work, Hg^0 adsorption experiments were conducted for 2 h. Therefore, the integration time of Eq. (6) is 2 h. Eq. (4) was used to fit the experimental data at 150°C, as shown in Fig. 4. The adsorption kinetic parameters of Eq. (3) can be obtained: $q_e = 4774.57$ μg/g, $k_a = 9.81 \times 10^{-7}$ $m^3/(\mu g \cdot min)$. Therefore, $CuMn_2O_4$ sorbent has a higher Hg^0 adsorption capacity. Hg^0 adsorption kinetics on the $CuMn_2O_4$ surface can be expressed as:

$$q = 4774.57\left(1 - \exp\left(-9.81 C_{in} \cdot t \times 10^{-7}\right)\right) \tag{7}$$

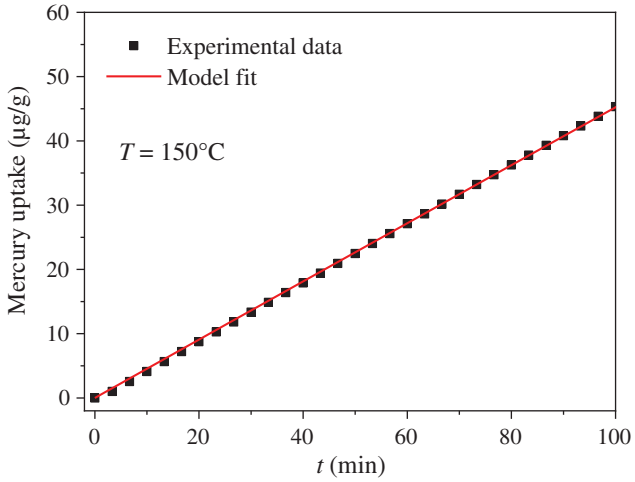

Figure 4: Model fitting and experimental data of Hg^0 adsorption amount of $CuMn_2O_4$ sorbent at 150°C

In order to further assess the accuracy and reliability of the adsorption kinetic model, Eq. (7) was used to predict the experimental results under the conditions of different reaction temperature. The comparison between the prediction results and experimental results at the reaction temperatures of 50, 100, 200, 250, 300 and 350°C is shown in Fig. 5. It can be seen that model predictions are in good agreement with the experimental results. Therefore, the kinetic model can accurately predict the Hg^0 adsorption amount of $CuMn_2O_4$ sorbent in a wide reaction temperature range.

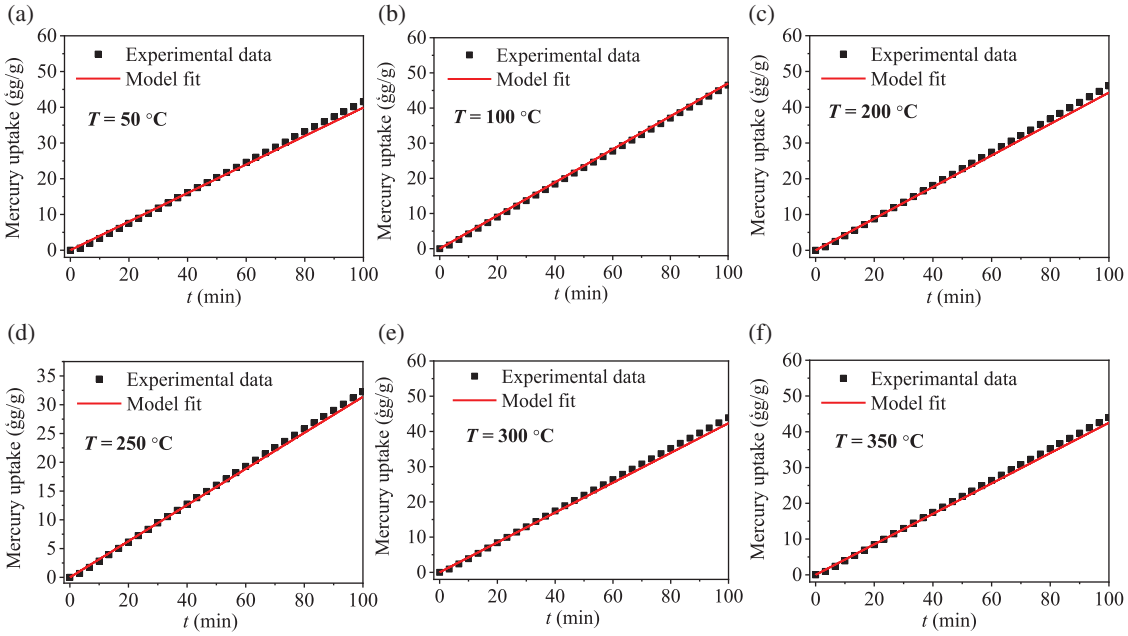

Figure 5: Comparison of experimental data and model predictions at different reaction temperatures: (a) 50°C, (b) 100°C, (c) 200°C, (d) 250°C, (e) 300°C, and (f) 350°C

3.3 Effect of HCl

HCl is the most important component for Hg^0 oxidation in flue gas [40]. Therefore, it is necessary to investigate the effect of HCl on Hg^0 transformation over $CuMn_2O_4$ sorbent. 10 ppm HCl was added to the simulated flue gas, Hg^0 removal efficiency of $CuMn_2O_4$ sorbent at different reaction temperatures is shown in Fig. 6. In general, HCl shows little effect on the Hg^0 removal efficiency of $CuMn_2O_4$ sorbent. It is well known that HCl can promote Hg^0 adsorption and oxidation in flue gas [41]. However, $CuMn_2O_4$ sorbent can show >95% Hg^0 removal efficiency in the absence of HCl. Therefore, Hg^0 removal efficiency of $CuMn_2O_4$ sorbent does not depend on the presence of HCl. Since $CuMn_2O_4$ sorbent shows excellent Hg^0 capture capacity and its Hg^0 removal efficiency does not depend on the presence of HCl, HCl has almost no effect on Hg^0 removal by $CuMn_2O_4$ sorbent. The slightly inhibitory effect (~1.2%) at 200°C and promotional effect (~1.3%) at 300°C of Fig. 6 are attributed to the experimental error rather than the effects of HCl. Although HCl has little effect on Hg^0 removal efficiency of $CuMn_2O_4$ sorbent, HCl may affect the mercury speciation on the $CuMn_2O_4$ surface.

To further explore the effect of HCl on the mercury speciation over the $CuMn_2O_4$ surface, TPD experiments were carried out to identify the mercury speciation. The TPD curves of the used $CuMn_2O_4$ sorbent after Hg^0 removal experiments in the absence and presence of HCl are shown in Fig. 7. After Hg^0 removal experiments in the absence of HCl, the used $CuMn_2O_4$ sorbent only showed a peak at 385°C (Fig. 7a). This peak is attributed to the decomposition of yellow HgO species [42].

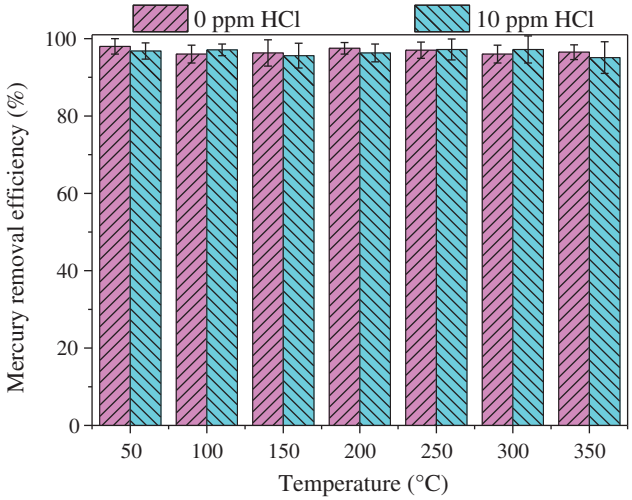

Figure 6: Effect of HCl on Hg^0 removal efficiency of $CuMn_2O_4$ in the temperature range of 50–350°C

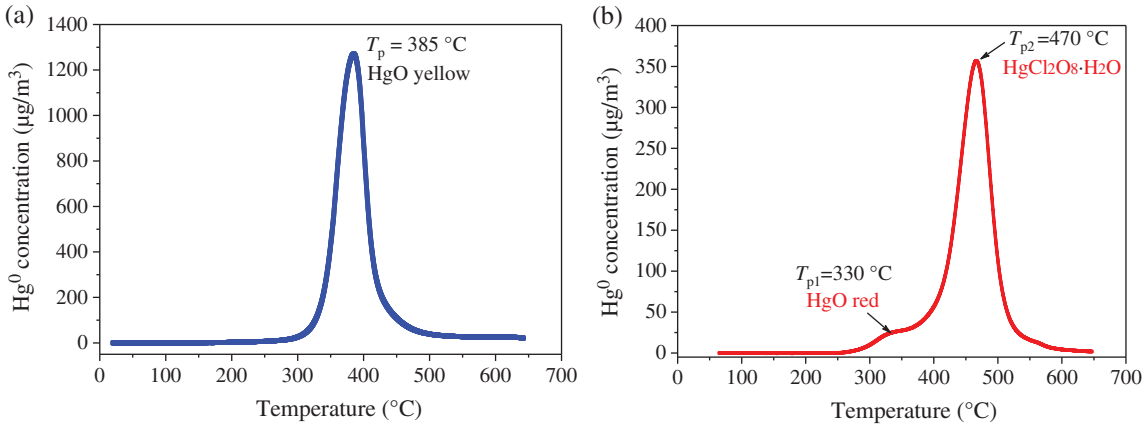

Figure 7: Temperature-programmed desorption curves of the used $CuMn_2O_4$ sorbent after Hg^0 removal experiments in the (a) absence and (b) presence of HCl

However, after Hg^0 removal experiments in the presence of HCl, there are two peaks at 330°C and 470°C in the TPD curve of the used $CuMn_2O_4$ sorbent (Fig. 7b). The TPD peak at 330°C is attributed to the decomposition of red HgO species adsorbed on the sorbent surface. Yellow HgO and red HgO have different crystal structure, leading to the different decomposition temperature. The desorption peak at 470°C is ascribed to the decomposition of $HgCl_2O_8{\cdot}H_2O$ species [42].

Therefore, mercury species adsorbed on the $CuMn_2O_4$ surface in the presence of HCl mainly exist in the forms of HgO and $HgCl_2O_8{\cdot}H_2O$.

XPS analysis was further applied to illustrate the effect of HCl on the Hg^0 transformation on $CuMn_2O_4$ sorbent surface. It can be seen in Fig. 8 that the peak of Hg 4f XPS spectra is observed at 104.61 eV. This is characteristic of Hg $4f_{5/2}$ spin-orbit doublet of Hg^{2+}. This suggests that Hg^0 is chemisorbed and transformed into oxidized mercury species (Hg-Cl compounds) on $CuMn_2O_4$ sorbent surface. Therefore, it can be inferred that Hg-Cl compounds are formed on $CuMn_2O_4$ sorbent in the presence of HCl.

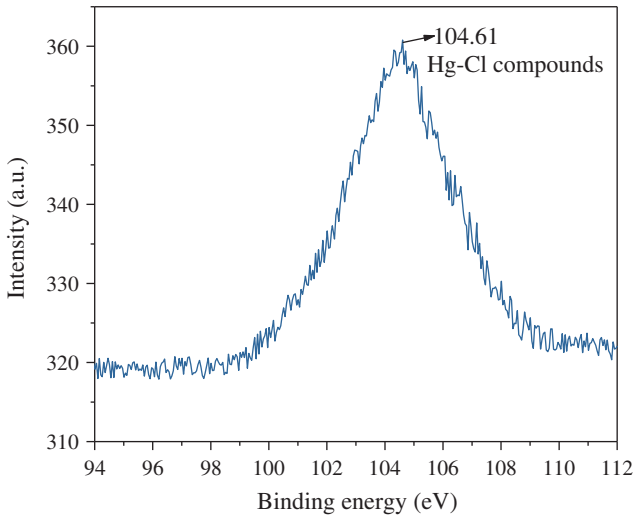

Figure 8: Hg 4f XPS spectra of used $CuMn_2O_4$ sorbent

The performance of $CuMn_2O_4$ sorbent depends on the surface chemistry reactions. The overall process of Hg^0 adsorption on $CuMn_2O_4$ sorbent in the presence of HCl is controlled by three steps. Firstly, Hg^0 is chemically adsorbed on $CuMn_2O_4$ sorbent surface. Then, HgO is formed through the oxidation reaction of Hg^0(ads) with chemisorbed oxygen on $CuMn_2O_4$ sorbent surface. Finally, HCl reacts with the adsorbed HgO to form Hg-Cl compound ($HgCl_2O_8{\cdot}H_2O$) on $CuMn_2O_4$ surface. The adsorption mechanism of Hg^0 transformation on $CuMn_2O_4$ sorbent in the presence of HCl can be described by the following three chemical reactions [43]:

$$Hg^0 + \text{catalyst} \rightarrow Hg^0(\text{ads}) \tag{8}$$

$$Hg^0(\text{ads}) + O(s) \rightarrow HgO(\text{ads}) \tag{9}$$

$$HgO(\text{ads}) + HCl + O(s) \rightarrow HgCl_2O_8.H_2O(s) \tag{10}$$

The formation of $HgCl_2O_8{\cdot}H_2O$ species is governed by Eq. (10). The area of $HgCl_2O_8{\cdot}H_2O$ desorption peak is much larger than that of HgO desorption peak, indicating that $HgCl_2O_8{\cdot}H_2O$ is the main mercury specie on the used $CuMn_2O_4$ sorbent surface. Based on the above TDP analysis, it can be found that the presence of HCl shows a larger effect on the mercury speciation over the $CuMn_2O_4$ sorbent surface.

4 Conclusions

Experiments were conducted to investigate the effect mechanism of HCl on Hg^0 transformation over $CuMn_2O_4$ sorbent. $CuMn_2O_4$ sorbent is a mesoporous material, and has a good thermal stability at high temperatures during Hg^0 removal. The mesopores are favorable for mass transfer during Hg^0 capture. $CuMn_2O_4$ sorbent shows >95% Hg^0 removal efficiency in the wide temperature range of 50–350°C. The excellent Hg^0 removal performance of $CuMn_2O_4$ sorbent is closely associated with the electron-transfer environment caused by the mixed valence states of Cu and Mn cations. The equilibrium adsorption capacity and adsorption rate constant are 4774.57 μg/g and 9.81×10^{-7} $m^3/(\mu g \cdot min)$, respectively. The developed kinetic model can well predict Hg^0 adsorption over $CuMn_2O_4$ sorbent. The Hg^0 removal performance of $CuMn_2O_4$ sorbent is independent on the presence of HCl. Mercury species adsorbed on the used $CuMn_2O_4$ sorbent in the presence of HCl mainly exist in the forms of HgO and $HgCl_2O_8 \cdot H_2O$. HCl shows a larger effect on mercury speciation over $CuMn_2O_4$ sorbent.

Funding Statement: This work was supported by National Key R&D Program of China (2016YFB0600604), National Natural Science Foundation of China (52006083), and Fundamental Research Funds for the Central Universities (2019kfyRCPY021).

Conflicts of Interest: The authors declare that they have no conflicts of interest to report regarding the present study.

References

1. Hower, J. C., Senior, C. L., Suuberg, E. M., Hurt, R. H., Wilcox, J. L. et al. (2010). Mercury capture by native fly ash carbons in coal-fired power plants. *Progress in Energy and Combustion Science, 36(4),* 510–529. DOI 10.1016/j.pecs.2009.12.003.
2. Frandsen, F., Dam-Johansen, K., Rasmussen, P. (1994). Trace elements from combustion and gasification of coal—An equilibrium approach. *Progress in Energy and Combustion Science, 20(2),* 115–138. DOI 10.1016/0360-1285(94)90007-8.
3. Zhao, S., Pudasainee, D., Duan, Y., Gupta, R., Liu, M. et al. (2019). A review on mercury in coal combustion process: Content and occurrence forms in coal, transformation, sampling methods, emission and control technologies. *Progress in Energy and Combustion Science, 73,* 26–64. DOI 10.1016/j.pecs.2019.02.001.
4. Back, S. K., Lee, E. S., Seo, Y. C., Jang, H. N. (2020). The effect of NaOH for the recovery of elemental mercury from simulated mixture wastes and waste sludge from an industrial process using a thermal desorption process. *Journal of Hazardous Materials, 384,* 121291. DOI 10.1016/j.jhazmat.2019.121291.
5. Sung, J. H., Back, S. K., Jung, B. M., Kang, Y. S., Lee, C. G. et al. (2017). Speciation and capture performance of mercury by a hybrid filter in a coal-fired power plant. *International Journal of Coal Geology, 170,* 35–40. DOI 10.1016/j.coal.2016.10.008.
6. Li, H., Zu, H., Yang, Z., Yang, J., Xu, H. et al. (2021). The adsorption mechanisms of Hg^0 on marcasite-type metal selenides: The influences of metal-terminated site. *Chemical Engineering Journal, 406,* 126723. DOI 10.1016/j.cej.2020.126723.
7. Yang, Z., Li, H., Yang, Q., Qu, W., Zhao, J. et al. (2020). Development of selenized magnetite ($Fe_3O_{4-x}Se_y$) as an efficient and recyclable trap for elemental mercury sequestration from coal combustion flue gas. *Chemical Engineering Journal, 394,* 125022. DOI 10.1016/j.cej.2020.125022.
8. Xu, Y., Luo, G., Pang, Q., He, S., Deng, F. et al. (2019). Adsorption and catalytic oxidation of elemental mercury over regenerable magnetic Fe-Ce mixed oxides modified by non-thermal plasma treatment. *Chemical Engineering Journal, 358,* 1454–1463. DOI 10.1016/j.cej.2018.10.145.

9. Yang, Y., Liu, J., Wang, Z. (2020). Reaction mechanisms and chemical kinetics of mercury transformation during coal combustion. *Progress in Energy and Combustion Science, 79,* 100844. DOI 10.1016/j.pecs.2020.100844.
10. Wu, Q., Wang, S., Liu, K., Li, G., Hao, J. (2018). Emission-limit-oriented strategy to control atmospheric mercury emissions in coal-fired power plants toward the implementation of the minamata convention. *Environmental Science & Technology, 52(19),* 11087–11093. DOI 10.1021/acs.est.8b02250.
11. Yang, Y., Liu, J., Zhang, B., Liu, F. (2017). Density functional theory study on the heterogeneous reaction between Hg^0 and HCl over spinel-type $MnFe_2O_4$. *Chemical Engineering Journal, 308,* 897–903. DOI 10.1016/j.cej.2016.09.128.
12. Rodríguez-Pérez, J., López-Antón, M. A., Díaz-Somoano, M., García, R., Martínez-Tarazona, M. R. (2013). Regenerable sorbents for mercury capture in simulated coal combustion flue gas. *Journal of Hazardous Materials, 260,* 869–877. DOI 10.1016/j.jhazmat.2013.06.026.
13. Xu, Y., Luo, G., Zhou, M., Zhang, Q., Li, Z. et al. (2021). Natural ferruginous manganese ore for efficient immobilization of elemental mercury from coal combustion flue gas. *Fuel, 283,* 118946. DOI 10.1016/j.fuel.2020.118946.
14. Li, H., Feng, S., Qu, W., Yang, J., Liu, S. et al. (2018). Adsorption and oxidation of elemental mercury on chlorinated ZnS surface. *Energy & Fuels, 32(7),* 7745–7751. DOI 10.1021/acs.energyfuels.8b01188.
15. Qu, W., Liu, J., Shen, F., Wei, P., Lei, Y. (2016). Mechanism of mercury-iodine species binding on carbonaceous surface: Insight from density functional theory study. *Chemical Engineering Journal, 306,* 704–708. DOI 10.1016/j.cej.2016.07.115.
16. Yang, Z., Yang, J., Li, H., Qu, W., Leng, L. et al. (2020). Advances in magnetically recyclable remediators for elemental mercury degradation in coal combustion flue gas. *Journal of Materials Chemistry A, 8(36),* 18624–18650. DOI 10.1039/D0TA06311H.
17. Zhang, B., Liu, J., Dai, G., Chang, M., Zheng, C. (2015). Insights into the mechanism of heterogeneous mercury oxidation by HCl over V_2O_5/TiO_2 catalyst: Periodic density functional theory study. *Proceedings of the Combustion Institute, 35(3),* 2855–2865. DOI 10.1016/j.proci.2014.06.051.
18. Wang, Y., Shen, B., He, C., Yue, S., Wang, F. (2015). Simultaneous removal of NO and Hg^0 from flue gas over Mn–Ce/Ti-pILCs. *Environmental Science & Technology, 49(15),* 9355–9363. DOI 10.1021/acs.est.5b01435.
19. Wang, Z., Liu, J., Zhang, B., Yang, Y., Zhang, Z. et al. (2016). Mechanism of heterogeneous mercury oxidation by HBr over V_2O_5/TiO_2 catalyst. *Environmental Science & Technology, 50(10),* 5398–5404. DOI 10.1021/acs.est.6b00549.
20. He, C., Shen, B., Chi, G., Li, F. (2016). Elemental mercury removal by CeO_2/TiO_2-PILCs under simulated coal-fired flue gas. *Chemical Engineering Journal, 300,* 1–8. DOI 10.1016/j.cej.2016.04.017.
21. Yang, Y., Liu, J., Wang, Z., Zhang, Z. (2017). Homogeneous and heterogeneous reaction mechanisms and kinetics of mercury oxidation in coal-fired flue gas with bromine addition. *Proceedings of the Combustion Institute, 36,* 4039–4049. DOI 10.1016/j.proci.2016.08.068.
22. van Otten, B., Buitrago, P. A., Senior, C. L., Silcox, G. D. (2011). Gas-phase oxidation of mercury by bromine and chlorine in flue gas. *Energy & Fuels, 25(8),* 3530–3536. DOI 10.1021/ef200840c.
23. Yang, Y., Liu, J., Liu, F., Wang, Z., Ding, J. (2018). Comprehensive Hg/Br reaction chemistry over Fe_2O_3 surface during coal combustion. *Combustion and Flame, 196,* 210–222. DOI 10.1016/j.combustflame.2018.06.018.
24. Wo, J., Zhang, M., Cheng, X., Zhong, X., Xu, J. et al. (2009). Hg^{2+} reduction and re-emission from simulated wet flue gas desulfurization liquors. *Journal of Hazardous Materials, 172(2),* 1106–1110. DOI 10.1016/j.jhazmat.2009.07.013.
25. Yang, Y., Liu, J., Zhang, B., Liu, F. (2017). Mechanistic studies of mercury adsorption and oxidation by oxygen over spinel-type $MnFe_2O_4$. *Journal of Hazardous Materials, 321,* 154–161. DOI 10.1016/j.jhazmat.2016.09.007.
26. Zhou, Q., Lei, Y., Liu, Y., Tao, X., Lu, P. et al. (2018). Gaseous elemental mercury removal by magnetic Fe–Mn–Ce sorbent in simulated flue gas. *Energy & Fuels, 32(12),* 12780–12786. DOI 10.1021/acs.energyfuels.8b03445.

27. Zheng, Y., Jensen, A. D., Windelin, C., Jensen, F. (2012). Review of technologies for mercury removal from flue gas from cement production processes. *Progress in Energy and Combustion Science, 38(5),* 599–629. DOI 10.1016/j.pecs.2012.05.001.
28. Zhang, Z., Wu, J., Li, B., Xu, H., Liu, D. (2019). Removal of elemental mercury from simulated flue gas by ZSM-5 modified with Mn-Fe mixed oxides. *Chemical Engineering Journal, 375,* 121946. DOI 10.1016/j.cej.2019.121946.
29. Shoemaker, D. P., Li, J., Seshadri, R. (2009). Unraveling atomic positions in an oxide spinel with two jahn−Teller ions: Local structure investigation of $CuMn_2O_4$. *Journal of the American Chemical Society, 131(32),* 11450–11457. DOI 10.1021/ja902096h.
30. Lamb, A. B., Scalione, C. C., Edgar, G. (1922). The preferential catalytic combustion of carbon monoxide in hydrogen. *Journal of the American Chemical Society, 44(4),* 738–757. DOI 10.1021/ja01425a007.
31. Tanaka, Y., Utaka, T., Kikuchi, R., Takeguchi, T., Sasaki, K. et al. (2003). Water gas shift reaction for the reformed fuels over Cu/MnO catalysts prepared via spinel-type oxide. *Journal of Catalysis, 215(2),* 271–278. DOI 10.1016/S0021-9517(03)00024-1.
32. Yang, Y., Liu, J., Du, X., Ding, J., Liu, F. (2020). Metal–metal interactions of ternary spinel for efficient NH_3 selective catalytic reduction of NO_x at a low temperature. *Energy & Fuels, 34(12),* 15424–15432. DOI 10.1021/acs.energyfuels.0c02293.
33. Yang, Y., Liu, J., Liu, F., Wang, Z., Ding, J. et al. (2019). Reaction mechanism for NH_3-SCR of NO_x over $CuMn_2O_4$ catalyst. *Chemical Engineering Journal, 361,* 578–587. DOI 10.1016/j.cej.2018.12.103.
34. Wang, Z., Liu, J., Yang, Y., Yu, Y., Yan, X. et al. (2020). Regenerable $Co_xMn_{3-x}O_4$ spinel sorbents for elemental mercury removal from syngas: Experimental and DFT studies. *Fuel, 266,* 117105. DOI 10.1016/j.fuel.2020.117105.
35. Yang, Y., Liu, J., Wang, Z., Long, Y., Ding, J. (2019). Interface reaction activity of recyclable and regenerable Cu-Mn spinel-type sorbent for Hg^0 capture from flue gas. *Chemical Engineering Journal, 372,* 697–707. DOI 10.1016/j.cej.2019.04.177.
36. Wang, Z., Liu, J., Yang, Y., Yu, Y., Yan, X. et al. (2020). AMn_2O_4 (A = Cu, Ni and Zn) sorbents coupling high adsorption and regeneration performance for elemental mercury removal from syngas. *Journal of Hazardous Materials, 388,* 121738. DOI 10.1016/j.jhazmat.2019.121738.
37. Yang, Y., Liu, J., Wang, Z., Zhang, Z., Ding, J. et al. (2019). Nature of active sites and an oxygen-assisted reaction mechanism for mercury capture by spinel-type $CuMn_2O_4$ sorbents. *Energy & Fuels, 33(9),* 8920–8926. DOI 10.1021/acs.energyfuels.9b01696.
38. Wang, Z., Liu, J., Yang, Y., Yu, Y., Yan, X. et al. (2020). Insights into the catalytic behavior of $lamno_3$ perovskite for Hg^0 oxidation by HCl. *Journal of Hazardous Materials, 383,* 121156. DOI 10.1016/j.jhazmat.2019.121156.
39. Davis, M. E. (2002). Ordered porous materials for emerging applications. *Nature, 417(6891),* 813–821. DOI 10.1002/chin.20040245.
40. Schofield, K. (2012). Mercury emission control from coal combustion systems: A modified air preheater solution. *Combustion and Flame, 159(4),* 1741–1747. DOI 10.1016/j.combustflame.2011.12.011.
41. Wilcox, J., Rupp, E., Ying, S. C., Lim, D. H., Negreira, A. S. et al. (2012). Mercury adsorption and oxidation in coal combustion and gasification processes. *International Journal of Coal Geology, 90,* 4–20. DOI 10.1016/j.coal.2011.12.003.
42. Rumayor, M., Diaz-Somoano, M., Lopez-Anton, M. A., Martinez-Tarazona, M. R. (2013). Mercury compounds characterization by thermal desorption. *Talanta, 114,* 318–322. DOI 10.1016/j.talanta.2013.05.059.
43. Yang, Y., Liu, J., Zhang, B., Zhao, Y., Chen, X. et al. (2017). Experimental and theoretical studies of mercury oxidation over CeO_2-WO_3/TiO_2 catalysts in coal-fired flue gas. *Chemical Engineering Journal, 317,* 758–765. DOI 10.1016/j.cej.2017.02.060.